

Time dependent photoionization opacities in dense Gamma–Ray Burst environments

Davide Lazzati¹, Rosalba Perna^{2,3} & Gabriele Ghisellini⁴

¹ *Institute of Astronomy, University of Cambridge, Madingley Road, Cambridge CB3 0HA, England*

² *Harvard Society of Fellows, 78 Mt. Auburn Street, Cambridge, MA 02138*

³ *Harvard–Smithsonian Center for Astrophysics, 60 Garden Street, Cambridge, MA 02138*

⁴ *Osservatorio Astronomico di Brera, via Bianchi 46, 23807 Merate (LC), Italy*

e-mail: lazzati@ast.cam.ac.uk

26 October 2018

ABSTRACT

The recent detection of a transient absorption feature in the X–ray prompt emission of GRB 990705 showed the importance of such observations in the understanding of gamma–ray bursts and their progenitors. We investigate the time dependence of photoionization edges during the prompt emission of bursts in different environments. We show that their variability can be used to infer the density and geometry of the surrounding medium, giving important clues to unveil the nature of the burst progenitor.

Key words: Gamma–rays: bursts — X–rays: general — X–rays: ISM — line: formation

1 INTRODUCTION

The nature of the progenitors of gamma–ray bursts (GRBs) is still mysterious, since the fireball producing the gamma–ray emission does not carry any information about the progenitor generating it (see, e.g., Piran 1999). Recent observations (e.g., Kulkarni et al. 1999) suggest the association of GRBs with the final stages of evolution of massive stars (Woosley 1993, Paczyński 1998; MacFadyen & Woosley 1999), but many crucial points still remain controversial. The possible evidence of rebrightening shown by the optical afterglows of several bursts ~ 30 days after the burst explosion (Bloom et al. 1999; Reichart 1999; Galama et al. 2000) suggests a simultaneous explosion of the burst with a Type Ic supernova. On the other hand, the detection of iron absorption and emission features in the X–ray emission of the bursts and afterglows (Amati et al. 2000; Piro et al. 2000) can be explained with a two–step explosion, in which the burst onset follows a supernova explosion by several months (Lazzati et al. 1999; Vietri et al. 2001; Lazzati et al. 2001).

These different scenarios can be distinguished through the analysis of the radial distribution of the interstellar medium surrounding the explosion site (Ghisellini et al. 1999). If the burst explodes simultaneously with the supernova, the photons propagate through the pre–explosion stellar wind, while in the two–step scenario a high density metal enriched supernova remnant is expected to surround the burst explosion site (Lazzati et al. 1999).

In this paper we study the variability properties of photoionization edges in the first several tens of seconds from the burst onset, for the different radial distributions of the

density profile characterizing these two scenarios. Temporal variations of the opacities are indeed expected as a result of the gradual photoionization of the medium by the X–ray prompt emission of the burst. A similar variability effect on absorption lines had been discussed by Perna & Loeb (1998) and, in the X–rays, by Böttcher et al. (1999). In these papers, however, dependences on the radial profile of the density had not been considered.

The paper is organized as follows: in §2, we present some analytic approximations for the time–dependent opacities which hold for the optically thin case, discussed in §3. In §4, we present the results of the general (numerical) solution to the problem, and compare it with the analytic approximations derived in §2. In §5, we discuss possible effects of the fireball expansion in the absorbing medium. Finally, our results are summarized in §6.

2 ANALYTIC THEORY

Consider a distribution $n(r)$ of absorbers, characterized by a photoionization cross–section σ . In the case of an impulsive illumination by a strong ionizing flux the density $n(r)$ becomes time dependent, and so does the absorption opacity:

$$\tau(t) = \sigma \int_0^\infty n(r, t) dr \quad (1)$$

To solve Eq. 1, we must determine the time–dependent density $n(r, t)$. We use a particular time reference: at each radius r from the photon source, the time is set to be zero when the first ionizing photon passes by. By saying that the ionization

time at radius \tilde{r} is \tilde{t} , we then mean that \tilde{t} is the time interval between the first ionizing photon crossing the radius \tilde{r} and the complete ionization of all absorbing ions located at the same radius. The advantage of this time reference is that the travel time of photons is null, and the time t is also the time measured by an observer at infinity. The same conceptual scheme applies in §5 for the radius of the fireball.

Consider now a medium in which recombination is not efficient and let us neglect the change of the resonant frequency as an atom is progressively stripped off its electrons from the ground state to complete ionization. The first condition is easily fulfilled in GRBs, given their high ionization flux during the prompt phase (exceptions may however be possible, see Lazzati et al. 2001). In this case the density $n(r, t)$ remains constant until all electrons are stripped. The time of complete stripping depends on the distance r of an atom from the photon source. We assume that, at a given radius \tilde{r} , $n(\tilde{r}, t)$ changes abruptly in time:

$$n(\tilde{r}, t) = n(\tilde{r}) \chi_{[0, \tilde{Z} t_{\text{ion}}(\tilde{r})]}(t) \quad (2)$$

where $\chi_{[a, b]}(x) = 1$ for $a \leq x \leq b$ and 0 elsewhere, t_{ion} is the ionization time of a single electron and \tilde{Z} is the “efficient number” of electrons of the relative element. \tilde{Z} is in general smaller than the atomic number Z of the element, since other processes can contribute to ionization. These include collisional ionization, the Auger effect and the ionization of the external electrons by the UV flux. The actual value of \tilde{Z} can be obtained through numerical simulations and is not universal, being dependent on the ionizing UV continuum and the density of the absorbing medium (see § 4). The ionization time of a single electron is given by:

$$t_{\text{ion}} = \left[\int_{\nu_0}^{\infty} \frac{F(\nu)}{h\nu} \sigma(\nu) d\nu \right]^{-1} \quad (3)$$

where $F(\nu)$ is the flux of ionizing radiation at a given radius, taking into account the effect of absorption from material at lower radii. Eq. 3 modifies as:

$$\begin{aligned} t_{\text{ion}}(r) &= \frac{4\pi r^2}{\int_{\nu_0}^{\infty} \frac{L(\nu)}{h\nu} e^{-\tau(\nu)} \sigma(\nu) d\nu} = \\ &= \frac{4\pi r^2}{\int_{\nu_0}^{\infty} \frac{L(\nu)}{h\nu} e^{-\sigma(\nu)} \int_0^r n(\rho, t) d\rho \sigma(\nu) d\nu} \end{aligned} \quad (4)$$

where $L(\nu)$ is the luminosity of the ionizing continuum and ν_0 is the threshold photoionization frequency. Note that the ionization time, needed to compute the density of absorbers, depends on the density itself in a non-linear way. For this reason Eq. 4 does not have a general analytical solution.

3 OPTICALLY THIN MEDIA

If the absorbing medium is optically thin, the flux at a given radius does not depend (at least as a first approximation) on the absorption taking place at smaller radii. In this case Eq. 4 simplifies to:

$$t_{\text{ion}}(r) = \frac{4\pi r^2}{\int_{\nu_0}^{\infty} \frac{L(\nu)}{h\nu} \sigma(\nu) d\nu} \quad (5)$$

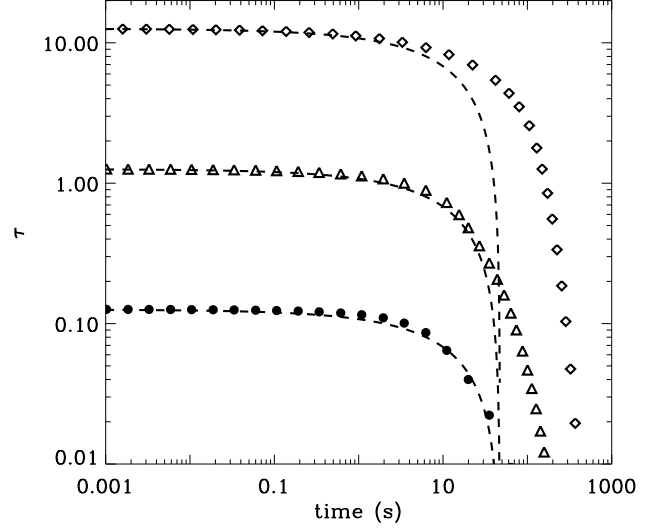


Figure 1. Opacity vs. time for a uniform cloud of absorbers. Initially opaque, intermediate and thin clouds are considered, from top to bottom (see text for the parameter set). The dashed lines correspond to the analytic approximations of Eq. 11, while the symbols are obtained with the numerical simulations described in §4. As expected, the analytic approximation holds in the optically thin regime, but fails to reproduce accurately the drop of the opacity in the optically thick cases (top line and diamonds).

By approximating the shape of a photoionization edge as $\sigma(\nu) = \sigma_0 (\nu/\nu_0)^{-3}$, and considering a power-law spectrum for the ionizing flux [$L(\nu) = L_0 (\nu/\nu_0)^{-\alpha}$], Eq. 5 becomes:

$$t_{\text{ion}}(r) = (3 + \alpha) h \frac{4\pi r^2}{L_0 \sigma_0} \quad (6)$$

Combining Eq. 6 with Eq. 1 and Eq. 2 we obtain:

$$\tau(\nu, t) = \sigma_0 \left(\frac{\nu}{\nu_0} \right)^{-3} \int_{R_{\text{if}}(t)}^{\infty} n(r) dr \quad (7)$$

where $R_{\text{if}}(t)$, the radius of the ionization front at time t , is obtained by inverting Eq. 6:

$$R_{\text{if}}(t) = \left(\frac{L_0 \sigma_0 t}{4\pi h \tilde{Z} (3 + \alpha)} \right)^{1/2} \quad (8)$$

Assuming an absorbing medium whose density decreases as a power law with distance, [$n(r) = n_0 (r/R_0)^{-\beta}$], we obtain

$$\tau(\nu, t) = \sigma_0 \left(\frac{\nu}{\nu_0} \right)^{-3} n_0 R_0^\beta \int_{\max[R_0, R_{\text{if}}(t)]}^{\max[R_M, R_{\text{if}}(t)]} r^{-\beta} dr \quad (9)$$

where R_M and R_0 are the maximum and minimum radii of the density profile. This avoids unphysical divergences at very large and very small radii. With this assumptions Eq. 9 becomes:

$$\begin{aligned} \tau(\nu, t) &= \sigma_0 n_0 R_0^\beta \left(\frac{\nu}{\nu_0} \right)^{-3} \times \\ &\times \begin{cases} \ln \left\{ \frac{\max[R_M, R_{\text{if}}(t)]}{\max[R_0, R_{\text{if}}(t)]} \right\} & \beta = 1 \\ \frac{\max[R_M, R_{\text{if}}(t)]^{1-\beta} - \max[R_0, R_{\text{if}}(t)]^{1-\beta}}{1-\beta} & \beta \neq 1 \end{cases} \end{aligned} \quad (10)$$

Two particularly interesting cases are a uniform distribution up to a given radius R_M and a rapidly decreasing ($\beta > 1$) distribution extending to infinity.

3.1 Uniform density

In the case of a uniform density of absorbers ($\beta = 0$), Eq. 10 becomes particularly simple:

$$\tau(\nu, t) = \sigma_0 n_0 \left(\frac{\nu}{\nu_0}\right)^{-3} \begin{cases} R_M - R_0 & R_{\text{if}} < R_0 \\ R_M - \sqrt{At} & R_0 < R_{\text{if}} < R_M \\ 0 & R_{\text{if}} > R_M \end{cases} \quad (11)$$

where A is given by:

$$A = \frac{L_0 \sigma_0}{4\pi h \tilde{Z} (3 + \alpha)} \quad (12)$$

Note that the case of uniform density can correspond not only to the case of a burst surrounded by a standard interstellar medium, but would also be a reasonable approximation for the case of a young supernova remnant (see Lazzati et al. 1999).

The opacity is constant at the beginning, then decays becoming rapidly negligible. Examples of this behavior are shown in Fig. 1 (dashed lines) for three different initial conditions: an opaque ($\tau(0) \sim 13$) cloud, an intermediate ($\tau(0) \sim 1.3$) cloud and a thin ($\tau(0) \sim 0.13$) cloud. We have considered the photoionization edge of iron, with a resonance cross section $\sigma_0 \sim 2 \times 10^{-20} \text{ cm}^2$ and a threshold frequency $h\nu = 9.28 \text{ keV}$. The parameterization adopted for the ionizing flux and the ambient medium is: $L_0 = 1.75 \times 10^{31} \text{ erg s}^{-1} \text{ Hz}^{-1}$, $\alpha = 0$ (similarly to the spectrum of GRB 990705, Amati et al. 2000), $R_0 = 10^{13} \text{ cm}$, $R_M = 1 \text{ pc}$ and $n_0 = 200, 20, 2 \text{ cm}^{-3}$, respectively. These conditions are quite extreme, since they correspond to a total mass of the absorbing iron of $\sim 1000, 100$ and $10 M_\odot$, respectively. On the other hand, a $\tau \sim 1$ feature lasting for ~ 10 seconds has indeed been detected (Amati et al. 2000), and very large iron masses are required, in some scenarios, to explain this feature (see Lazzati et al. 2001 and references therein for a more complete discussion).

We have considered in the simulation a constant ionizing luminosity. This is not generally true for GRBs, where fluctuations on timescales of fractions of seconds are usually observed. This would cause small scale fluctuations, with the same timescale, on the time evolution of the opacities, but the general trend is unaffected. Moreover, the burst may turn off before the complete ionization of the surrounding medium. In this case the results of this paper would hold only for times smaller than the turn off time of the GRB.

By comparison with the numerical simulations presented in §4 (where the approximations of §2 are released), the ‘‘efficient number’’ of electrons of iron in these conditions turns out to be $\tilde{Z}_{\text{Fe}} \sim 7$. The dashed lines have been computed adopting this value.

In Fig. 2, we show the time of complete ionization of the iron ions as a function of the distance from the source of the ionizing photons. In the analytic approximation of Eq. 8, this time does not depend on the initial opacity and density distribution of the medium.

3.2 Decaying density profiles

Let us consider now the case of a density profile decreasing with distance from the burst source. This can correspond, for example, to a pre-explosion stellar wind if the bursts are

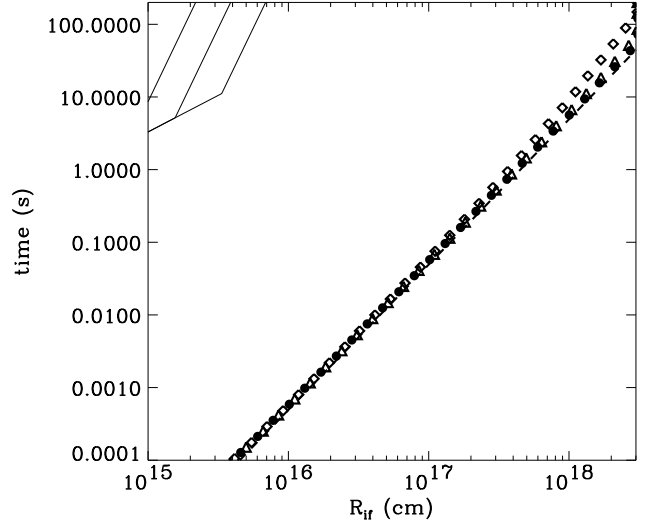


Figure 2. Time of complete ionization vs. radius for the same geometrical setup of Fig. 1. The dashed line shows the analytic approximation of Eq. 8. The symbols refer to the same cases of Fig. 1. Since in the simulations the approximation of the step function (Eq. 2) is not used, the symbols are relative to the time at which the fraction of iron completely ionized is a half of the total. The thin solid lines in the upper left corner of the figure show the time at which the fireball crosses the radius R_{if} (see §5). Since this time is always much larger than the time of ionization, the hydrodynamics of the fireball does not influence the evolution of the opacity.

associated with the death of massive stars. In this case we would have $\beta = 2$ (Chevalier & Li, 1999).

If the density of the absorbing medium decreases with distance sufficiently rapidly ($\beta > 1$), the maximum radius can be set to infinity and Eq. 10 becomes:

$$\tau(\nu, t) = \frac{\sigma_0 n_0 R_0^\beta \left(\frac{\nu}{\nu_0}\right)^{-3}}{\beta - 1} \begin{cases} R_0^{1-\beta} & R_{\text{if}} < R_0 \\ (At)^{\frac{1-\beta}{2}} & R_{\text{if}} > R_0 \end{cases} \quad (13)$$

where A is given in Eq. 12. After a short initial constant phase, the opacity decreases in time as a power-law whose slope depends only on the index β of the density profile. The time evolution of the opacity in a wind environment is shown in Fig. 3. We used $R_0 = 10^{13} \text{ cm}$ and initial densities $n_0 = 10^9, 10^8$ and 10^7 cm^{-3} (corresponding to $\tau(0) \sim 200, 20$ and 2). The parameters describing the ionization flux are the same used for Fig. 1. In Fig. 4, we show the time evolution of the radius of complete ionization, for the same parameters used for Fig. 3.

4 NUMERICAL RESULTS

To solve the problem in its full generality, we remove the approximations made in § 2. We start the simulation at $t = 0$, and let the burst photons propagate. In propagating from a point at position r to another point at position $r + \Delta r$, the ionizing flux is reduced according to:

$$F_\nu(r + \Delta r, t + \Delta t) = F_\nu(r, t) \exp[-\Delta\tau_\nu(r, t)] \frac{r^2}{(r + \Delta r)^2}. \quad (14)$$

The optical depth due to photoabsorption within the distance Δr is then given by:

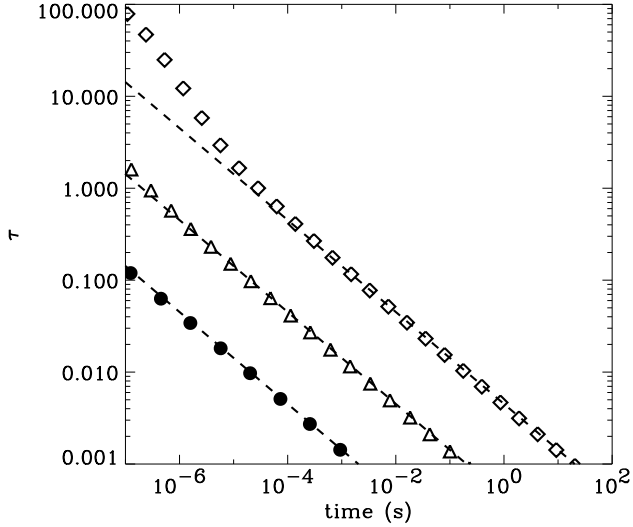


Figure 3. Opacity vs. time for a wind environment. Initially opaque, intermediate and thin winds are considered, from top to bottom (see text for the parameter set). The dashed lines correspond to the analytic approximations of Eq. 13, while the symbols are obtained with the numerical simulations described in §4. As expected, the analytic approximation holds for $\tau < 1$.

$$\Delta\tau_\nu(r, t) = \Delta r \sum_j n_j(r, t) \sigma_j(\nu). \quad (15)$$

The photoionization cross sections are taken from Reilman & Manson (1979). The ionic concentrations are determined by solving the system of equations:

$$\begin{aligned} \frac{dn_j(r, t)}{dt} = & q_{j-2}n_{j-2} + q_{j-1}n_{j-1} + c_{j-1}n_{j-1}n_e \\ & - (q_j + c_j n_e + \alpha_j n_e)n_j + \alpha_{j+1}n_{j+1}n_e. \end{aligned} \quad (16)$$

The q_j and c_j are respectively the photoionization and collisional ionization coefficients of ion j , while α_j is the recombination coefficient. Note that q_{j-2} refers to inner shell photoionization followed by Auger ionization. The collisional ionization rates are calculated according to Younger (1981). We compute the terms due to photoionization by integrating $L_\nu \sigma_\nu$ numerically. The recombination rates are given by the sum of the radiative and dielectronic recombination rates. The code uses routines developed by Raymond (1979; see also Perna, Raymond & Loeb 2000 for a similar application and further details). After updating the ionization fractions at each time step Δt , the optical depth $\tau_\nu(t) = \int dr \Delta\tau_\nu(r, t)$ is recomputed.

A comparison between the numerical and analytical results is shown in Fig. 1, 2, 3 and 4. In all these figures, the analytical approximation is drawn as a dashed line, while the numerical results are overlaid as symbols (circles, diamonds and triangles). The introduction of recombination and collisional ionization does not change significantly the results with respect to the analytic case, where only photoionization is considered. As expected, corrections must be applied in the optically thick regime.

In Fig. 1, the opacity is dominated by material at large radii. The analytic approximation is valid when the initial opacity is small or intermediate ($\tau(0) \lesssim 1$), but underestimates the time of decline for an initially opaque cloud. For both the initially thin and thick cases, the analytic approx-

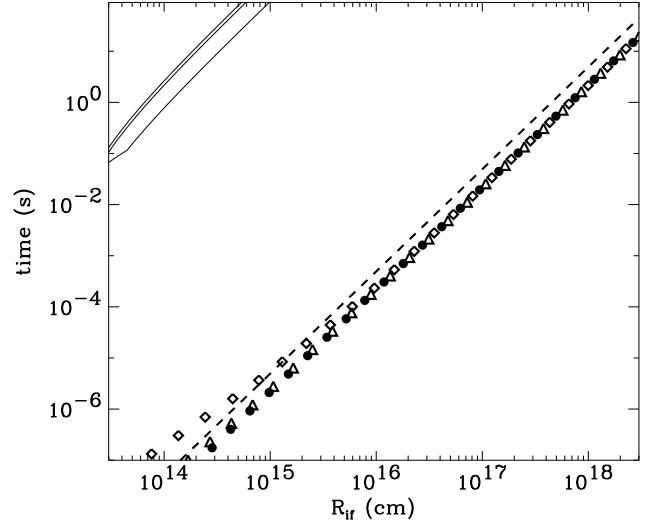


Figure 4. Same as Fig. 2 but for the wind environment of Fig. 3.

imation declines faster than the numerical result. This is due to the approximation of Eq. 2, which severely underestimates the absorption at a given radius for $t > t_{\text{ion}}(r)$.

Fig. 2 shows the time of complete ionization for the same parameter set of Fig. 1. In the numerical simulations the time of complete ionization is not a well defined quantity, since at each radius and at any time there is always the possibility (albeit very small) to have ions with bounded electrons. To properly compare with the time defined in Eq. 6, which is plotted as a dashed line, the symbols (circles, diamonds and triangles) show the time at which about 50 % of the iron is completely stripped (FeXXVII). The figure shows that the analytic approximation reproduces accurately the numeric results, with small deviations at large radii for the initially opaque case.

In the case of a wind environment (Fig. 3), the opacity is dominated by material at small radii. The analytic approximation describes accurately the temporal decay of the opacity in the optically thin and intermediate cases ($\tau(0) \lesssim 1$). For an initially optically thick medium, the numerical solution deviates at small times, but collapses onto the analytic approximation when the medium becomes optically thin. Again, $\bar{Z}_{\text{Fe}} \sim 7$ is adequate. The analytic time of complete ionization for a wind environment is compared with the results of numerical simulations in Fig. 4. Again, the analytic approximation is adequately accurate at all times but for the initially optically thick case, in which deviations are observed.

5 FIREBALL DYNAMICS

For all our calculations we have assumed that the ionization flux comes from a point source. This is not strictly true, since in the fireball model the prompt radiation is produced by the expanding shell. To check whether our assumption is reasonable we must demonstrate that the fireball radius is smaller than the ionization radius at all times.

The radius of the relativistic fireball expanding in

an inhomogeneous external medium is given by (see, e.g., Meszaros, Rees & Wijers, 1998):

$$R_{\text{fb}}(t) = R_{\text{IS}} + c\Gamma_0^2 \begin{cases} t & t \leq t_{\text{ES}} \\ \frac{3-\beta}{4-\beta} t^{\frac{1}{4-\beta}} & t > t_{\text{ES}} \end{cases}, \quad (17)$$

where Γ_0 is the asymptotic Lorentz factor of the fireball and $R_{\text{IS}} \sim 10^{13}$ cm is the internal shock radius, i.e. the radius at which the first ionizing photons are produced. The time t_{ES} is the onset time of external shocks, where the fireball expansion starts to be slowed down by the interaction with the external medium. This is given by (Meszaros, Rees & Wijers 1998):

$$t_{\text{ES}} = \left\{ \left[\frac{(3-\beta)E}{4\pi\Gamma_0^2 m_p c^2 n_{\{H,0\}}} + R_0^3 \right] R_0^{-\beta} \right\}^{\frac{1}{3-\beta}} \frac{1}{\Gamma_0^2 c}, \quad (18)$$

where E is the total fireball energy, m_p the proton mass, and a particle distribution $n_H(R) = n_{\{H,0\}}(r/R_0)^{-\beta}$ has been assumed. Note that the distribution of particles in the external medium follows the distribution of the absorbers given above. The normalization are instead different. For solar iron abundance we have $n_0 = 4.68 \times 10^{-5} n_{\{H,0\}}$ (Anders & Grevesse 1989).

In Fig. 2 and 4, the time at which the fireball crosses the radius R_{if} is plotted with thin solid lines. We assumed a fireball with $E = 10^{52}$ erg and $\Gamma_0 = 100$, and an iron abundance ten times solar. It can be seen that the fireball crossing time is always much larger than the time of ionization. We conclude that, for a reasonable set of parameters, the assumption of decoupling between the ionization and the hydrodynamics is valid.

6 CONCLUSIONS

We have calculated the time dependence of the absorption opacities due to the material in the surroundings of gamma-ray bursts. We have been able to qualitatively reproduce the numerical results with analytic expressions using some approximations appropriate for the optically thin regime.

In the optically thick regime, corrections must be applied. In the case of a uniform medium, the analytic expressions fail to reproduce exactly the lifetime of the absorption feature (i.e. the timescale of constant optical depth), while in the wind case the analytic expressions are in good agreement with the numerical results at all but the very early times.

An important issue is the observability of these features. On one hand, we require the density of the surrounding medium to be high, in order to have the highest possible opacity. On the other hand (Lazzati et al. 2001), the Thomson scattering optical depth, τ_T , of the absorbing material must be less than one, in order to maintain the flickering behavior of the γ -ray lightcurve. For a given Thomson opacity, the iron opacity is given by $\tau_{\text{Fe}} \sim 1.5\tau_T A_{\text{Fe}}$, where A_{Fe} is the iron abundance in solar units. Iron enriched media are hence necessary to observe a deep iron feature in a $\tau_T \lesssim 0.1$ cloud. Enriched media around GRBs have indeed been observed (Amati et al. 2000; Lazzati et al. 2001).

For the wind environment, the absorption feature has an extremely short lifetime, not detectable with the present and near future detectors and instruments. It then appears

that a stellar wind, even if strong and appropriate to a very massive progenitor, is not able to imprint a detectable absorption feature in the X-ray spectrum of bursts. The reason is the immediate ionization of the absorbing material. However, there is still the possibility that the wind of the progenitor, especially in the last phases, is unsteady and intermittent, therefore populating the burst environment with a density profile different from R^{-2} and corresponding to more mass at larger radii than the case we assumed. If this case can be described by a larger value of R_0 , then the lifetime of the absorption feature should scale as R_0^2 and detectable features may appear if $R_0 \sim 10^{15}$ cm and/or with a weaker ionization flux, i.e. in X-ray poor bursts. If, beyond R_0 , the density profile retains a power law profile, then also the absorption optical depth decreases in time as a power law, and this discriminates the wind case from the uniform density scenario, where the fall off of the absorption feature should be more abrupt.

The required time resolved X-ray spectroscopic observations are beyond the capabilities of present instruments and satellites, which can provide only a time integrated measurement of the opacity on timescales of $5 \div 10$ seconds (cfr. Amati et al. 2000). The Swift satellite, however, will be able to slew on target and to start the observations with the X-ray telescope in a few seconds (in particularly favorable cases), and will be sensitive enough to measure time-resolved opacities (Perna et al., in preparation).

REFERENCES

- Amati L. et al., 2000, *Science*, 290, 953
 Anders, E., & Grevesse, N. 1989, *Geochim. Cosmochim. Acta*, 53, 197
 Bloom J. S. et al., 1999, *Nat.*, 401, 453
 Böttcher M., Dermer C. D., Crider A. W., Liang E. P. 1999, *A&A*, 343, 111
 Chevalier R. A., Li, Z., 1999, *ApJ*, 520, L29
 Galama T. J. et al., 2000, *ApJ*, 536, 185
 Ghisellini G., Haardt F., Campana S., Lazzati D., Covino S., 1999, *ApJ*, 517, 168
 Kulkarni S. R. et al., 1999, in *Proceedings of the 5th Huntsville Gamma-Ray Bursts Symposium*, Eds. Kippen R. M., Mallozzi R. S., Fishman G. J., AIP conference proceedings 526
 Lazzati D., Campana S., Ghisellini G., 1999, *MNRAS*, 304, L31
 Lazzati D., Ghisellini G., Amati L., Frontera F., Vietri M., Stella L., 2001, *ApJ* in press
 MacFadyen, A. L., & Woosley, S. E. 1999, *ApJ*, 524, 262
 Meszaros P., Rees M. J., Wijers R. A. M. J., 1998, *ApJ*, 499, 301
 Paczyński, B. 1998, *ApJ*, 494, L45
 Perna R., Loeb, A., 1998, *ApJ*, 501, 467
 Perna R., Raymond J., Loeb A., 2000, *ApJ*, 533, 658
 Piran T., 1999, *Phys. Rep.*, 314, 575
 Piro L. et al., 2000, *Science*, 290, 955
 Raymond J. C., 1979, *ApJS*, 39, 1
 Reichart D. E., 1999, *ApJ*, 521, L111
 Reilman R. F., Manson S. T., 1979, *ApJS*, 40, 815
 Vietri M., Ghisellini G., Lazzati D., Fiore F., Stella L., 2001, *ApJ*, 550, L43
 Younger S. M., 1981, *JQSRT*, 26, 329
 Woosley, S. E. 1993, *ApJ*, 405, 273